Fully Coriolis-Coupled Quantum Studies of the H + O_2 ($v_i = 0-2$, $j_i = 0,1$) → OH + O Reaction on an Accurate Potential Energy Surface: Integral Cross Sections and Rate Constants

Shi Ying Lin,[†] Zhigang Sun,[‡,#] Hua Guo,[*,†] Dong Hui Zhang,[‡] Pascal Honvault,[£] Daiqian Xie,[§] and Soo-Y. Lee[#]

Department of Chemistry and Chemical Biology, University of New Mexico, Albuquerque, New Mexico 87131, Center for Theoretical and Computational Chemistry, and State Key Laboratory of Molecular Reaction Dynamics, Dalian Institute of Chemical Physics, Chinese Academy of Sciences, Dalian 116023, China, Institut UTINAM, UMR CNRS 6213, University of Franche-Comté, Campus de la Bouloie, UFR Sciences et Techniques, 25030 Besançon cedex, France, Institute of Theoretical and Computational Chemistry, Laboratory of Mesoscopic Chemistry, School of Chemistry and Chemical Engineering, Nanjing University, Nanjing 210093, China, and Division of Chemistry & Biological Chemistry, School of Physical & Mathematical Science, Nanyang Technological University, Singapore 637616

Received: October 9, 2007

We present accurate quantum calculations of the integral cross section and rate constant for the H + O_2 → OH + O combustion reaction on a recently developed ab initio potential energy surface using parallelized time-dependent and Chebyshev wavepacket methods. Partial wave contributions up to $J = 70$ were computed with full Coriolis coupling, which enabled us to obtain the initial state-specified integral cross sections up to 2.0 eV of the collision energy and thermal rate constants up to 3000 K. The integral cross sections show a large reaction threshold due to the quantum endothermicity of the reaction, and they monotonically increase with the collision energy. As a result, the temperature dependence of the rate constant is of the Arrhenius type. In addition, it was found that reactivity is enhanced by reactant vibrational excitation. The calculated thermal rate constant shows a significant improvement over that obtained on the DMBE IV potential, but it still underestimates the experimental consensus.

I. Introduction

The H + O_2 → HO + O reaction is considered to be the single most important reaction in combustion chemistry due to its pivotal role in the chain-branching ignition in the oxidation of hydrogen and most hydrocarbons.[1] This reaction and its reverse are thought to proceed adiabatically on the ground electronic state potential energy surface (PES) of $HO_2(\tilde{X}^2A'')$, which is dominated by a deep HO_2 well (∼2.38 eV from the H + O_2 asymptote). The reaction path has no intrinsic barrier other than the endothermicity of ∼0.7 eV.[2] The large endothermicity results in low reactivity, which coupled with the radical nature of the products makes experimental measurements very difficult.

A key quantity studied in this work is the thermal rate constant for the H + O_2 reaction. Because of its importance in modeling ignition and flame propagation, experimental measurements of the rate constant have been reported in several temperature ranges by many groups,[3−6] and the results have been summarized in several reviews.[7,8] On the theoretical side, the rate constant has been calculated using the transition-state theory[9−11] and other statistical methods,[12,13] approximate quantum approaches,[14−18] as well as quasi-classical trajectory (QCT) methods.[11,19−24] Among them, the quantitative accuracy of the QCT method is questionable, particularly at low temperatures, although it helped to shed much light on the reaction dynamics. This is because the QCT results depend sensitively on how the zero-point energy (ZPE) is handled,[25,26] which becomes important when reactive trajectories possess less vibrational energy than the product ZPE. On the other hand, statistical methods also need validation because of the nonstatistical behaviors of this system observed in QCT[10,11,27,28] and quantum calculations.[29]

It is instructive to point out that the quantum reaction threshold of the title reaction is about 0.23 eV above the classical one, thanks to the large ZPE of the OH product. For this and other reasons, the reaction dynamics should be treated quantum mechanically if an unambiguous characterization is to be achieved. However, an exact quantum dynamic calculation of the system is very challenging because of the large number of quantum states supported by the HO_2 well, and because of the dominance of long-lived resonances above the reaction threshold.[30−32] These difficulties are further exacerbated by the floppiness of the HO_2 intermediate complex, which renders the commonly used centrifugal sudden (CS) approximation[33,34] or the *J*-shifting model[35] inaccurate.[36,37] Until now, only a few quantum calculations have been carried out with full Coriolis coupling,[36−40] and none have reported the rate constant. In addition, nonadiabatic effects might play a role in strong interaction regions[41] as well as in the dissociation asymptotes.[42,43] The inclusion of the nonadiabatic couplings further adds to the complexity of the treatment.

Besides the thermal rate constant, several measurements of the integral cross section (ICS) for the title reaction have been

* To whom correspondence should be addressed.
† University of New Mexico.
‡ Chinese Academy of Sciences.
£ UFR Sciences et Techniques.
§ Nanjing University.
# Nanyang Technological University.

10.1021/jp7098637 CCC: $40.75
Published on Web 01/09/2008

reported.[39,44−46] Unfortunately, inconsistencies were found due apparently to the experimental difficulties associated with the low reactivity. For instance, it has been claimed that a sharp increase of ICS occurs near the collision energy of 1.8 eV.[44,46] However, this feature could be verified by neither a latter experiment[39] nor theory.[26,38,40] The most recent theory−experiment comparison showed that the quantum ICS was significantly lower than the experimental data, and the discrepancy was attributed to the inaccuracies of the PES used in the calculation.[39]

An important factor in the accurate characterization of the title reaction is the PES. Much effort has been devoted to the development of a global PES for the $HO_2(\tilde{X}^2A'')$ system from ab initio data.[12,21,22,28,47−53] Among the existing PESs, the double many-body expansion (DMBE) IV PES of Varandas and coworkers[28] has enjoyed widespread popularity in the past decade,[10,11,16,17,26,30,32,36−38,40,54,55] thanks to its reasonable and balanced representation of the global properties of the PES. However, the accuracy of the DMBE PES has recently been questioned by several authors.[10,12,18,21,39] Given the fact that only a relatively small number of ab initio points were included, there is much room for improvement.

In an effort to advance our understanding of the HO_2 system, Xu, Xie, Zhang, Lin, and Guo (XXZLG) have, in 2005, reported a new PES for $HO_2(\tilde{X}^2A'')$ based on ∼15000 symmetry-unique ab initio points obtained using the Davidson corrected internally contracted multireference configuration interaction method (icMRCI+Q) with a large (aug-cc-pVQZ) basis set.[56] Subsequently, the ab initio points have also been fit to analytic forms using the reproducing kernel Hilbert space method.[57] The high quality of the XXZLG PES is manifested by a dramatically improved agreement with experimental vibrational frequencies, from errors of roughly 100 cm^{-1} on the DMBE IV PES to less than 10 cm^{-1} on the new XXZLG PES.[56] Recent calculations on the new XXZLG PES have also uncovered many significant differences in spectroscopic[58,59] and dynamic attributes[60,61] with the DMBE PES. Specifically, our $J = 0$ reactive scattering calculations for the title reaction[60] revealed that the direct channel identified on the DMBE IV PES, responsible for the elevated reaction probability above $E_c = 1.2$ eV,[30,36] is likely an artifact. These findings underscore the inadequacy of the semiempirical DMBE IV PES in dynamic studies and call for a reexamination of the reaction dynamics.

Toward that goal, we have recently reported preliminary results[29] on both the differential cross section (DCS) and ICS for the title reaction on the new XXZLG PES.[56] The state-resolved DCSs were obtained just above the reaction threshold, using a time-independent quantum method.[62] The dominance of both the forward and backward scattering peaks supports the notion that a long-lived reaction intermediate is involved. On the other hand, the ICS, obtained using a wavepacket method, increases monotonically with the collision energy above the reaction threshold, showing a near complete washout of the sharp resonance features in the reaction probabilities. However, the ICS was only reported up to the collision energy of 1.0 eV because the partial waves above $J = 50$ were not computed. In this article, we extended our earlier work by reporting the calculation of the ICS up to 2.0 eV with $J_{max} = 70$ and the rate constant up to 3000 K. In addition, we examined the influence of reactant rotational and vibrational excitation on the reactivity. The dynamic calculations were carried out on the XXZLG PES using a two different but fully Coriolis-coupled wavepacket methods. Such a study is highly desirable because it not only directly tests the accuracy of the PES but also provides a valuable benchmark for approximate methods. This publication is organized as follows. In section II, the fundamental theory and numerical aspects are briefly outlined. In section III, results are presented and discussed, and conclusions are summarized in section IV.

II. Theory

Our dynamic studies ignored the electronic and spin angular momenta of both the reactants and products and all nonadiabatic couplings, including those among the fine structure states of the reactants and products. Following our recent work,[29] we used the reactant (H + O_2) Jacobi coordinates (R,r,γ) in the calculations. Such a coordinate system allows the adaptation of the exchange symmetry between the two oxygen atoms, cutting the grid/basis size by half. The Hamiltonian is expressed in atomic units as

$$\hat{H} = -\frac{1}{2\mu_R}\frac{\partial^2}{\partial R^2} - \frac{1}{2\mu_r}\frac{\partial^2}{\partial r^2} + \frac{\hat{j}^2}{2\mu_r r^2} + \frac{\hat{l}^2}{2\mu_R R^2} + V(R,r,\gamma) \quad (1)$$

where r and R are, respectively, the diatomic (O−O) and atom−diatom (H−O_2) distances, with μ_r and μ_R as the corresponding reduced masses; $\hat{j}$ denotes the diatomic rotational angular momentum operator and $\hat{l}$ the orbital angular momentum operator. We can further express $\hat{l}^2$ as

$$\hat{l}^2 \equiv (\hat{J} - \hat{j})^2 = \hat{J}^2 + \hat{j}^2 - 2\hat{J}_z\hat{j}_z - \hat{J}_+\hat{j}_- - \hat{J}_-\hat{j}_+ \quad (2)$$

in which $\hat{J}$ and $\hat{j}$ are, respectively, the total and diatomic angular momentum operators with $\hat{J}_z$ and $\hat{j}_z$ as their projections onto the body-fixed (BF) z axis and $\hat{J}_+(\hat{J}_-)$ and $\hat{j}_+$ ($\hat{j}_-$) are the corresponding raising (lowering) operators. Here, the BF z axis is chosen to coincide with the $\vec{R}$ vector (R-embedding). The last two terms in eq 2, which are ignored in the CS approximation, represent the Coriolis coupling.[33,34] Because of the floppiness of the HO_2 system, the Coriolis terms were treated exactly in our calculations, allowing the scrambling of the helicity states. As a result, no dynamical approximation was introduced for the Hamiltonian in eq 1. In this work, $V(R,r,\gamma)$ is a spline fit of the recently modified XXZLG data set.[57]

Two wavepacket methods have been used in our calculations. The first is the time-dependent method based on the split-operator propagator. Since this method has been widely used in studying reaction dynamics,[63] including complex-forming reactions,[30,64] we concentrate here on the other wavepacket method based on the Chebyshev propagator.[65] To that end, the initial wavepacket ($|\psi_0\rangle$) was propagated using the modified Chebyshev recursion relation[66,67]

$$|\psi_{k+1}\rangle = D(2\hat{H}_{norm}|\psi_k\rangle - D|\psi_{k-1}\rangle) \quad k \geq 1 \quad (3)$$

where $|\psi_1\rangle = D\hat{H}_{norm}|\psi_0\rangle$. The normalized Hamiltonian, $\hat{H}_{norm} = (\hat{H} - H^+)/H^-$, was defined in terms of the spectral width and mean of the Hamiltonian, $H^{\pm} = (H_{max} \pm H_{min})/2$, with H_{max} (H_{min}) as the upper (lower) spectral bound.[68] The damping term (D) was introduced to enforce outgoing boundary conditions

$$D(x) = \begin{cases} 1 & \text{for } x \leq x_d \\ e^{-d_x(x-x_d)^2} & \text{for } x > x_d \end{cases} \quad (x = R,r) \quad (4)$$

Since the Chebyshev wavepacket propagation bears many similarities with time propagation,[69,70] it has been advanced by several authors for studying reaction dynamics.[66,67,71−74] Like the time-dependent approach,[63] reaction probabilities can be obtained at all energy points with a single propagation. The Chebyshev approach is considered to be more accurate because

it avoids the interpolation errors in approximating the exponential time propagator.[68] Another advantage of the Chebyshev wavepacket method is that real arithmetic can be used, as long as the initial wavepacket is chosen to be a real function.[70]

To propagate the wavepacket, the Hamiltonian was discretized using a mixed FBR/DVR (finite basis representation/discrete variable representation)[75] scheme. For R and r, equidistant grids were defined and labeled by α_1 and α_2. For the angular degrees of freedom, the following parity (p)-adapted BF-FBR was used as described in our earlier work[76]

$$|j\Omega;Jp\rangle = (2+2\delta_{\Omega,0})^{-1/2}(|J\Omega\rangle|j\Omega\rangle + p(-1)^J|J-\Omega\rangle|j-\Omega\rangle) \quad (5)$$

where $|j\Omega\rangle \equiv \Theta_{j\Omega}(\gamma,0)$ are normalized associate Legendre functions with the Condon−Shortley phase convention[77] and $|J\Omega\rangle = \sqrt{((2J+1)/8\pi^2)}D^{J^*}_{\Omega,0}$ represents the overall rotation, where $D^J_{\Omega,M}$ is the Wigner rotation matrix.[78] The projection of J and j onto the z axis in the BF frame, Ω, is thus restricted to be non-negative. To summarize, the wavepacket with a total angular momentum J and parity p was expressed as

$$|\psi^{Jp}\rangle = \sum_{\alpha_1\alpha_2 j\Omega} \Psi^{Jp}_{\alpha_1\alpha_2 j\Omega}|\alpha_1\rangle|\alpha_2\rangle|j\Omega;Jp\rangle \quad (6)$$

To evaluate the action of the kinetic energy operators (KEOs), we took advantage of the pseudospectral transformation between FBR and DVR. For example, the action of the first two KEO terms in eq 1 was calculated using fast sine Fourier transform (sine FFT). Since the third KEO term in eq 1 is diagonal in the BF-FBR, as shown below, its calculation is straightforward

$$\langle j'\Omega';Jp|\hat{j}^2|j\Omega;Jp\rangle = j(j+1)\delta_{j',j}\delta_{\Omega',\Omega} \quad (7)$$

The fourth KEO term in eq 1 could also be calculated using BF-FBR, where the operator is tri-diagonal

$$\langle j'\Omega';Jp|\hat{l}^2|j\Omega;Jp\rangle = [J(J+1)+j(j+1)-2\Omega^2]\delta_{j',j}\delta_{\Omega',\Omega} - [(1+\delta_{\Omega',0})(1+\delta_{\Omega,0})]^{-1/2}\{\lambda^+_{J\Omega}\lambda^+_{j\Omega}\delta_{\Omega',\Omega+1} + \lambda^-_{J\Omega}\lambda^-_{j\Omega}[\delta_{\Omega',\Omega-1} + p(-1)^J\delta_{\Omega',-\Omega+1}]\}\delta_{j',j} \quad (8)$$

where $\lambda^{\pm}_{jm} = \sqrt{j(j+1)-m(m\pm1)}$.

However, a drawback of the BF-FBR is that the spectral range is unmanageable when the corresponding rotational energy constant becomes very large, which happens near $R \approx 0$. To circumvent this problem, the wavepacket in the BF-FBR $|j\Omega;Jp\rangle$ was first transformed to the space-fixed (SF) frame FBR $|jl;Jp\rangle$ using the following formula[63]

$$|j\Omega;Jp\rangle = \sum_l (-1)^{j-l+\Omega}\sqrt{(2-\delta_{\Omega,0})(2l+1)}\begin{pmatrix} j & l & J \\ \Omega & 0 & -\Omega \end{pmatrix}\Big|jl;Jp\rangle \quad (9)$$

where (:::) denotes the 3-j symbol. Because the fourth KEO term is diagonal in the SF-FBR, the spectral range can be easily controlled by truncating the rotational energy. After applying the truncated rotational KEOs, the wave function was transformed back to the original BF-FBR. The computational efficiency was little effected using this scheme, compared to the direct calculation using eq 8.

Finally, the wavepacket was transformed to a grid where the action of the potential energy operator (the fifth term in eq 1) is diagonal. In this case, the angular DVR was defined by the angular Gauss−Legendre quadrature points associated with rotational basis $|j\Omega\rangle$. The angular DVR and FBR are related through a pseudospectral transform[79,80]

$$T^{(\Omega)}_{j\beta} = \sqrt{w_\beta}\,\Theta_{j\Omega}(\gamma_\beta) \quad (10)$$

where β denotes the index of the Gauss−Legendre quadrature points for the Jacobi angular coordinate and w_β is the corresponding weight.

In this work, the initial wavepacket was chosen as a product of a well-defined rovibrational eigenfunction $|\varphi_{v_ij_i}\rangle$ of O_2, a one-dimensional Gaussian-shaped wavepacket along the translational coordinate ($g(R) = Ne^{-(R-R_i)^2/2\delta^2}\cos k_0R$), and a SF angular momentum eigenstate in the coupled representation ($|JMj_il_i\rangle$)

$$|\psi_0\rangle = g(R)|\varphi_{v_ij_i}\rangle|JMj_il_i\rangle \quad (11)$$

where k_0, R_i, and δ are its mean momentum, mean position, and width, respectively, and N is the normalization constant.

The total reaction probabilities were obtained by calculating the outgoing flux at a reasonably large r using the following expression[81,82]

$$P(E) = \frac{1}{2\pi\mu_r|a_i(E)|^2(H^-)^2\sin^2\theta} \times \mathrm{Im}\left\langle \sum_k (2-\delta_{k0})e^{-ik\theta}\psi_k \middle| \sum_{k'}(2-\delta_{k'0})e^{-ik'\theta}\left[\delta(r-r_f)\frac{\partial}{\partial r}\psi_{k'}\right]\right\rangle \quad (12)$$

where $r = r_f$ defines the dividing surface in the product channel and $\theta \equiv \arccos((E - H^+)/H^-)$. $a_i(E)$ is the energy amplitude given by $a_i(E) = \langle i\sqrt{(\mu_R k_i/2\pi)}Rh_{l_i}^{(2)}(k_iR)|g(R)\rangle$,[73] where $h_{l_i}^{(2)}(k_iR)$ is the spherical Hankel function of the second kind.[83] The use of the Hankel function instead of the plane wave function allowed us to place the initial wavepacket at a sufficiently small R without worrying about the long-range centrifugal energy, as long as the interaction potential was zero. This approach has been successfully applied to a number of complex-forming reactions.[76,84]

The initial state (v_ij_i) specified ICS is then obtained by a partial wave summation over J and an average over l_i ($= |J - j_i|, ..., J + j_i$) of initial state ($v_ij_il_i$)-specified reaction probabilities

$$\sigma_{v_ij_i}(E) = \frac{f\pi}{(2j_i+1)k^2_{v_ij_i}}\sum_{J,l_i}(2J+1)P^J_{v_ij_il_i}(E) \quad (13)$$

where $k^2_{v_ij_i} = 2\mu_R E_c$, E_c is the collision energy, f is the electronic degeneracy factor which is 1/3 for the title reaction, and $P^J_{v_ij_il_i}(E)$ is the initial state ($v_ij_il_i$)-specified total reaction probability for the partial wave J, obtained from eq 12. For the convenience of discussion in the next section, we introduce the partial cross section defined as below

$$\sigma^J_{v_ij_i}(E) = \frac{\pi(2J+1)}{(2j_i+1)k^2_{v_ij_i}}\sum_{l_i}P^J_{v_ij_il_i}(E) \quad (14)$$

The ICS defined in eq 13 can thus be expressed as

$$\sigma_{v_ij_i}(E) = f\sum_J \sigma^J_{v_ij_i}(E) \quad (15)$$

Integration of the ICS over the collision energy with the Boltzmann weight led to the initial state-specified rate constant as given by

$$k_{v_i j_i}(T) = \frac{1}{k_B T}\left(\frac{8}{\pi \mu_R k_B T}\right)^{1/2} \int_0^\infty \sigma_{v_i j_i}(E_c) e^{-E_c/k_B T} E_c dE_c \qquad (16)$$

where k_B is the Boltzmann constant and T is temperature. The thermal rate constant can then be obtained by the Boltzmann average over various initial states.

III. Results and Discussion

A. Details of Calculations. We report here accurate quantum mechanical results of the ICSs and rate constants for the title reaction for various initial states, namely, ($v_i = 0, j_i = 1$), ($v_i = 0, j_i = 0$), ($v_i = 1, j_i = 0$), and ($v_i = 2, j_i = 0$). It should be noted that $j_i = 0$ represents an unphysical state because of the spin symmetry of O_2, but it was included to help us to understand the influence of reactant internal excitation on reactivity. Note that the calculation of the ICS for $j_i = 0$ reduces the computational costs to 1/3 of that for $j_i = 1$, where three initial wavepackets corresponding to $l_i = |J - 1|, J, |J + 1|$ are needed.

The quantum calculations were rather challenging primarily due to the requirement of a large basis/grid and a large number of partial waves. Specifically, partial waves up to $J_{max} = 50$ were needed to converge the ICS up to $E_c = 1.0$ eV, and $J_{max} = 70$ was needed for $E_c = 2.0$ eV. These high-J partial waves require extensive computational resources. To facilitate the calculations, we parallelized the Chebyshev wavepacket propagation using OpenMP, primarily for the matrix−vector multiplication. Linear scaling up to 16 nodes was achieved on a shared-memory IBM P5 machine at the High Performance Computing Center at University of New Mexico. Similar parallelization schemes were used for the time-dependent wavepacket propagation.

To determine the optimal numerical parameters, we carried out extensive convergence tests with the $J = 0$ Hamiltonian for the initial state of $O_2(v_i = 0, j_i = 1)$. The chosen parameters were employed for $J > 0$ calculations and for other initial states as well. For the $j_i = 0$ initial states, however, the even permutation symmetry and even rotational states were taken instead of odd symmetry and odd states for the $j_i = 1$ state. The final parameters are summarized as follows: $N_R = 79$ over $R \in (0.1, 9.5) a_0$; $N_r = 167$ over $r \in (0.5, 9.1) a_0$; $j = 1, 3, ..., 79$ (or $= 0, 2, 4, ..., 78$ for the $j_i = 0$ initial states) and $N_\gamma = 40$ over $\gamma \in (0, 90°)$; $R_i = 6.0 a_0$, $k_0^2/2\mu_R = 0.8$eV, and $\delta = 0.2 a_0$ for the initial wavepacket; $R_d = 7.0 a_0$ and $d_R = 0.01 a_0^{-2}$ for damping along R; $r_d = 7.1 a_0$ and $d_r = 0.01 a_0^{-2}$ for the damping along r; $r_f = 7.0 a_0$ for the dividing surface; and energy cut-offs of 0.2 Hartree for the PES and each KEO term. Finally, all allowed values of the helicity quantum number Ω ($\Omega = 0 - J$) were included in the Hamiltonian, and 15 000 steps of Chebyshev recursion were found to converge the results. A somewhat larger grid was used in the time-dependent wavepacket calculation. This difference is responsible for the negligible discrepancy between the calculated results ($J = 25$, $l_i = 24$) shown in the upper panel of Figure 1.

B. Reaction Probabilities and Coriolis Coupling. Due to space limitations, we only display several representative reaction probabilities for the initial state $O_2(v_i = 0, j_i = 1)$ in the upper panel of Figure 1. As the figure shows, the $J = 0$ probability has a significant reaction threshold due apparently to the quantum endothermicity of the reaction. It is also highly oscillatory, especially at low collision energies. These oscillations can be attributed to metastable resonance states supported by the deep HO_2 potential well. As already mentioned in our previous publication,[60] the $J = 0$ reaction probability decreases somewhat with the collision energy, in contrast to the DMBE IV PES on which the reaction probability increases substantially above $E_c = 1.2$ eV.[30,32] The latter feature has been attributed to the opening of a direct channel on the DMBE IV PES, which is apparently absent on the ab initio XXZLG PES. However, this difference makes little impact to the ICS because the $J = 0$ partial wave has a very small weight in the opacity function.

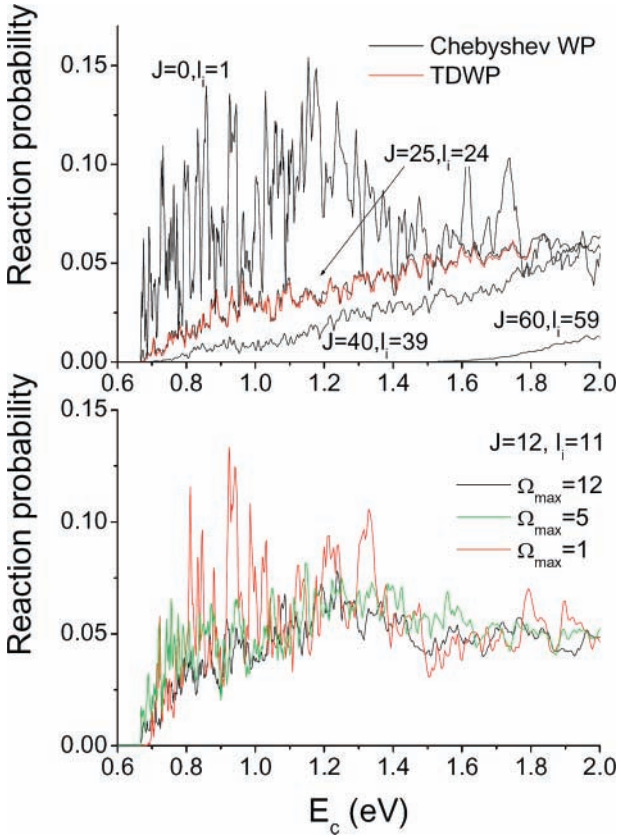

Figure 1. Upper panel: Energy dependence of the initial state ($v_i = 0, j_i = 1$)-specified reaction probability for several selected total angular momentum quantum numbers. The results obtained from the time-dependent wavepacket (TDWP, red line) and Chebyshev wavepacket (black line) calculations are compared for $J = 25$, $l_i = 24$. Lower panel: Comparison of the $J = 12$, $l_i = 11$ probability obtained with different Ω_{max} values.

For nonzero J values, the reaction threshold moves to higher collision energies due to the additional centrifugal barrier in the O + OH channel. Initially, the threshold increases with J very slowly because of the long-range attractive potential in the product channel. At high J values, the shift accelerates due partly to the quadratic J dependence of the centrifugal barrier and partly to a "submerged" barrier at a small O−OH distance in the product channel. It is also interesting to note that the $J > 0$ reaction probabilities typically increase with the collision energy and have less oscillations, consistent with the earlier observation of Meijer and Goldfield on the DMBE IV PES.[36−38] We note in passing that the $J > 0$ probabilities bear little resemblance to that for $J = 0$, indicating the inadequacy of the J-shifting model for the title reaction. The overall behaviors of reaction probabilities for other initial states are quite similar.

In the same figure, we compare the results obtained from the time-dependent and Chebyshev wavepacket calculations for $J = 25$, $l_i = 24$. The excellent agreement between two

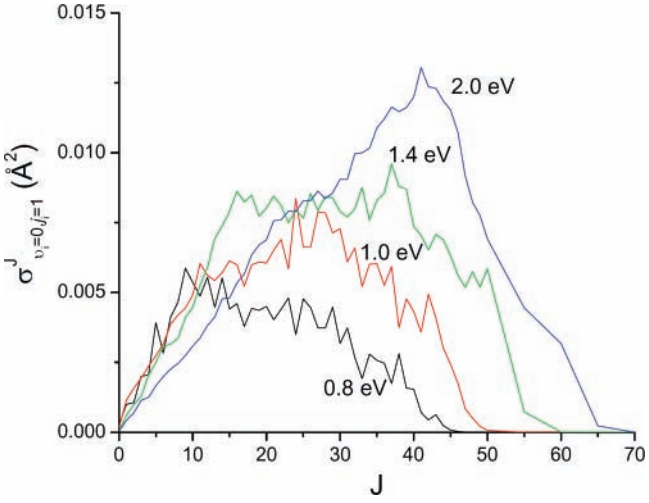

Figure 2. The $(2J + 1)$ weighted partial cross section for the initial state $(v_i = 0,j_i = 1)$-specified ICS at several collision energies.

independent calculations using different propagation schemes shown here and found for other angular momentum quantum numbers testifies to the reliability of the results.

In the lower panel of Figure 1, we illustrate the importance of the Coriolis coupling using $J = 12$, $l_i = 11$ as an example. As the figure shows, the approximation with $\Omega_{max} = 1$ is very poor for the title reaction. This observation is a direct result of the floppiness of the HO_2 intermediate. Including five helicity channels ($\Omega_{max} = 5$) in the model improves the agreement with the exact result ($\Omega_{max} = 12$), but it is still not accurate enough. An interesting observation is that the probabilities with truncated helicity blocks show stronger oscillations than the exact result, presumably because the Coriolis coupling reduces the lifetime of the resonance states. Our results are consistent with the earlier observations on the Coriolis coupling made by Meijer and Goldfield on the DMBE IV PES.[36−38]

C. Opacity Function and Interpolation in *J* Space. The $(2J + 1)$-weighted partial cross section for the initial state O_2-$(v_i = 0,j_i = 1)$ is displayed in Figure 2 for several collision energies. The opacity function typically rises with J initially and then decays, thanks to the competition between the degeneracy factor of $2J + 1$ and the shifting of the centrifugal barrier. As shown, the $J = 0$ contribution to the ICS is very small. As a result, attempts to describe the reaction in terms of the $J = 0$ reaction probability should be discouraged. As discussed above, the barrierless nature of the title reaction leads to a large number of partial waves. Even at an energy slightly above the reaction threshold ($E_c = 0.8$ eV), J values up to 45 were needed to converge the ICS. Classically, it means that the reaction takes place for a large range of the impact parameter. Some small oscillations are seen in the opacity function, presumably due to the oscillatory energy dependence of the reaction probabilities.

According to eq 15, the ICS is a sum of the J-dependent partial cross sections defined in eq 14. Because of the large number of partial waves included in the sum, the relatively small oscillations in the opacity function have only a limited impact on the accuracy of the highly averaged ICS and rate constant. Hence, the computational costs can be substantially reduced by interpolating the opacity function in the J space. Indeed, this has been suggested by Goldfield and Meijer and successfully applied to the title reaction.[38] To further test the viability of this idea, we compared in Figure 3 the exact result with all of the partial waves up to $J_{max} = 50$ to the approximate ICS, which was obtained with explicit partial waves for $J = 0-5$ followed

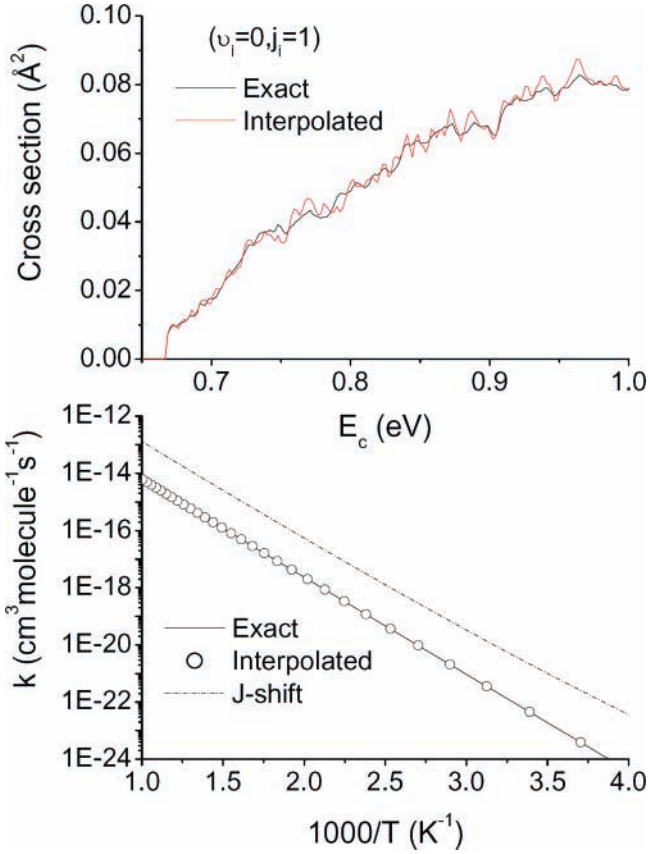

Figure 3. The initial state $(v_i = 0,j_i = 1)$-specified ICSs (upper panel) and rate constants (lower panel) obtained by exact partial wave summation and an interpolation method (see text for detail). The rate constant obtained from the *J*-shifting model is also included in the lower panel.

by interpolation with a $\Delta J = 5$ step. The agreement is excellent for the ICS and is even better for the rate constant after the Boltzmann averaging, shown in the lower panel of Figure 3. As a result of the excellent agreement, we report below the $(v_i = 0,j_i = 1)$ ICS obtained with a hybrid strategy in which all partial waves up to $J = 50$ were computed explicitly while higher J partial waves were obtained by interpolation from a J grid with an interval of five. For other initial states, the ICSs were obtained with all partial waves up to $J = 5$ followed by interpolation with $\Delta J = 5$.

D. Validity of the *J*-Shifting Model. In the lower panel of Figure 3, we have also compared the exact rate constant with that of a *J*-shifting model,[35] in which the $J > 0$ reaction probabilities were obtained approximately from the $J = 0$ result

$$P_i^J(E_c) \approx P_i^{J=0}(E_c - E_{shift}^J) \quad (17)$$

where E_{shift}^J is the energy shift of the J partial wave relative to $J = 0$, which was determined by the shift of the height of the effective barrier (PES + centrifugal potential) in the product channel. We assumed in eq 17 that the l components contribute equally.

It is clear from the lower panel of Figure 3 that the *J*-shifting model is inappropriate for the title reaction because it substantially overestimates the rate constant. The source of the errors can be traced back to the barrierless nature of the reaction, in which no unique transition state can be defined. Our results provided further support to the conclusion of Meijer and Goldfield[36,37] and call into question the reliability of results obtained with the *J*-shifting approximation.[15,18]

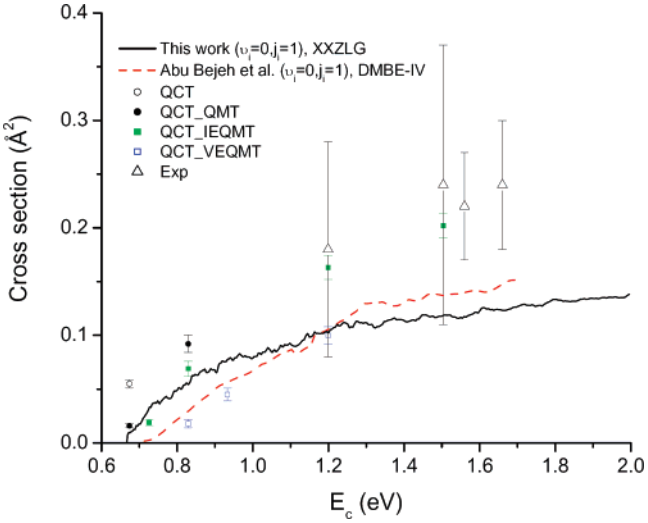

Figure 4. Comparison of the initial state ($v_i = 0,j_i = 1$)-specified ICSs obtained from wavepacket calculations on the XXZLG PES (this work) with the earlier quantum results on the DMBE IV PES.[38,39] These quantum results are also compared with ICSs from QCT calculations on the DMBE IV PES[26] and experimental measurements.[39]

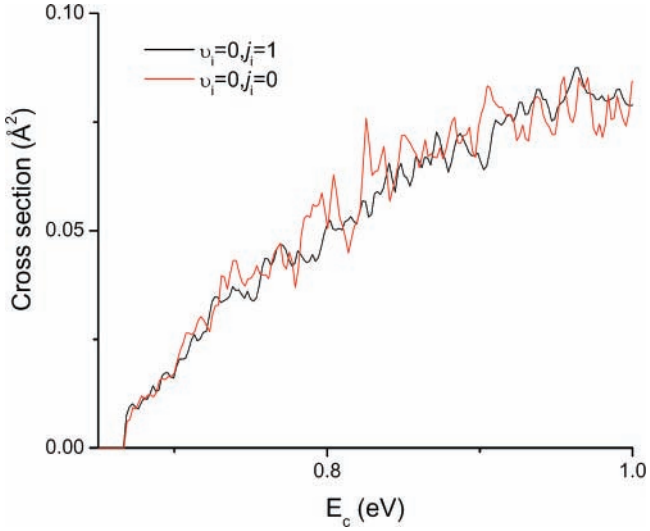

Figure 5. The initial state-specified ICSs for two different initial states, $v_i = 0,j_i = 1$and $v_i = 0,j_i = 0$.

E. Integral Cross Sections. In Figure 4, the initial state ($v_i = 0,j_i = 1$)-specified ICS is plotted against the collision energy and compared with available theoretical and experimental results.[39] The calculated ICS has a threshold at approximately 0.67 eV, which corresponds to the quantum endothermicity of the reaction. Above the threshold, the ICS increases near monotonically with the collision energy. Given the highly oscillatory structures of the reaction probabilities, the smooth nature of the excitation function is striking. It is apparent that the resonance structures were washed out by the partial wave summation, a typical observation for complex-forming reactions.

The monotonic increase of the ICS with the collision energy on the XXZLG PES is qualitatively similar to that on the DMBE IV PES, as reported by Goldfield and Meijer.[38,39] This similarity presumably reflects the fact that the overall reactivity of the title reaction is dominated by the OH + O product channel, where the two PESs are similar.[85] However, we would like to point out that recent state-resolved results clearly suggested that the two PESs produce quite different product state distributions,[60,61] underscoring the greater influence of the global PES on less-averaged scattering attributes. Quantitatively, the ICS on the XXZLG PES is larger below 1.2 eV of the collision energy, but the trend is reversed above that energy. In addition, the XXZLG PES has a lower classical threshold than the DMBE IV PES, as clearly seen in Figure 4.

The quantum ICS is also compared with the QCT results of Varandas on the DMBE IV PES,[26] who has extensively discussed various treatments of the large ZPE of the OH product. As shown in Figure 4, the differences between various ZPE treatments are quite significant, particularly near the reaction threshold, underscoring the inherent difficulties for treating the ZPE within the QCT framework. However, the trend in the quantum excitation function is reasonably reproduced by the QCT results. It appears that the QCT model with the best agreement with the quantum result is VEQMT (vibrational energy quantum mechanical threshold). QCT results have only been reported for the XXZLG PES with a zero impact parameter.[57]

The ultimate test of the calculated results is to compare them with experimental data. As shown in Figure 4, there is clearly no sudden increase of the calculated ICS near 1.8 eV as suggested by some earlier experiments.[44,46] In this aspect, our result is consistent with the recent experiment of Abu Bajeh et al.[39] and the theoretical results obtained by Goldfield and Meijer on the DMBE IV PES.[38] Quantitatively, the quantum ICS obtained from the XXZLG PES underestimates the experimental values, as in the case of the DMBE IV PES. In other words, the theory−experiment agreement is not much improved by the new PES. Although disappointing, there are several issues to consider. First of all, the experiments were very difficult to perform, and the results contain significant uncertainties, as evidenced by the large error bars in the figure. Second, the measurements[39] were not carried in jet-cooled conditions, and significant internal excitation in O_2 might exist. As discussed below, for example, the vibrational excitation in the O_2 reactant can considerably enhance the reactivity. On the theoretical side, there is always the question about the accuracy of the PES, despite the MRCI plus large basis set used in the ab initio calculations. In addition, the neglect of the nonadiabatic couplings could, in principle, alter the ICS. These issues should be examined in more detail in the future.

F. Influence of Reactant Rotation and Vibration. At high temperatures, many O_2 rovibrational states are populated. As a result, it is important to understand the roles of the reactant internal degrees of freedom in the reaction. A thorough examination of the influence of reactant rotational excitation on the ICS is prohibitively expensive for a wavepacket method because multiple wavepackets have to be launched for each J value. As a result, we restrict our discussion to the lowest rotational states of O_2. In Figure 5, we compare the ICSs for two initial states, namely, ($v_i = 0,j_i = 0$) and ($v_i = 0,j_i = 1$). As discussed above, the former is an unphysical state. As a result, the comparison is essentially an academic exercise. As shown in the figure, the reactant rotation makes very small differences in the ICS. However, the evidence is probably insufficient for us to conclude that the reactivity is not significantly effected by the reactant rotational excitation. In our earlier work using a time-independent quantum method, it was shown that the ICS decreases somewhat as j_i increases from 1 to 7, at least at low collision energies.[29]

Now let us turn to the influence of reactant vibration on the reactivity. To simplify the calculations, we approximated the $j_i = 1$ ICS using the $j_i = 0$ initial state, which reduced the computational costs by two-thirds. This approximation is justified by the results in Figure 5, namely, the ICSs for the

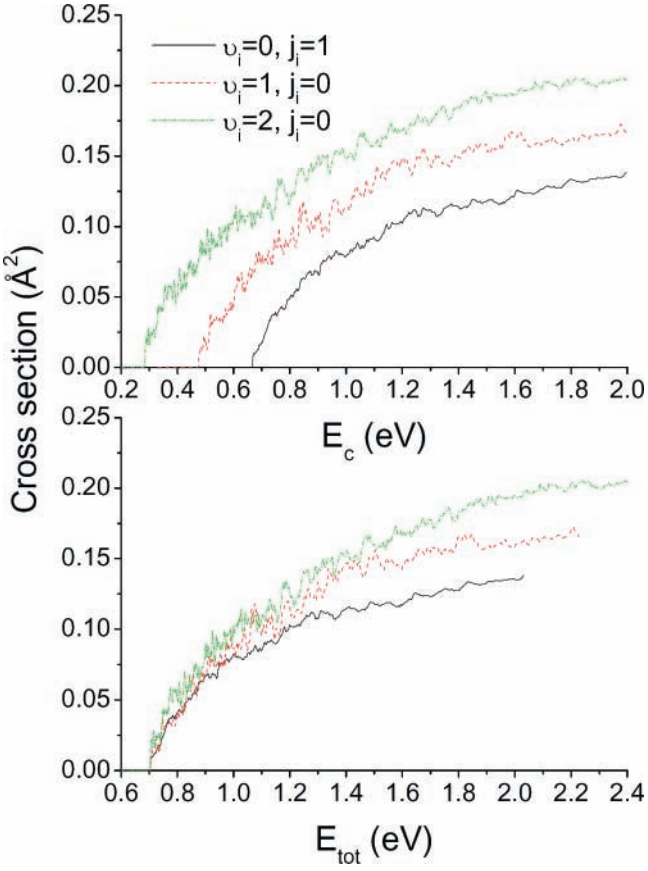

Figure 6. The initial state-specified ICSs, as a function of collision energy (upper panel) or total energy (lower panel), for different reactant vibrational sates.

two initial rotational states are essentially the same. Coupled with the interpolation over J discussed above, the approximate calculation of the ICS for vibrationally excited O_2 can be performed with less than one-tenth of the original computational costs. In Figure 6, three initial state-specified ICSs are compared. These $j_i = 0$ results were obtained by including all partial waves for $J < 6$ followed by interpolation over J with a $\Delta J = 5$ step. As the upper panel of the figure shows, initial vibrational excitation significantly reduces the threshold in the collision energy, underscoring the effectiveness of the vibrational degree of freedom in promoting the title reaction.

To gain more quantitative insights, we compare the ICSs as a function of total energy in the lower panel, which is defined in reference to the potential minimum of the H + O_2 channel. At most energies, there is a significant enhancement of the ICS when the O_2 molecule is vibrationally excited. In other words, the reactant vibrational energy is more effective in promoting the reaction than the translational energy. This feature has been noted in our earlier quantum work at low energies.[29] Similar observations have been made by Teitelbaum et al.[23] and by Dochovic and Parker[24] in their QCT studies on the DMBE IV PES. This should not come as a surprise as the title reaction features the O−O bond cleavage. Indeed, the barrierless nature of the PES can be considered as the ultimate case of a "late" transition state, in the language of Polanyi,[86] for which the reactant vibrational excitation is effective to push the system over the barrier. Interestingly, our recent studies of the HO_2 vibration demonstrated that the O−O overtones are highly organized all the way to the dissociation limit,[58,59] which might play a role in the vibrational enhancement of the reactivity of the title reaction. As discussed below, this property of the title reaction has an important implication in the rate constant.

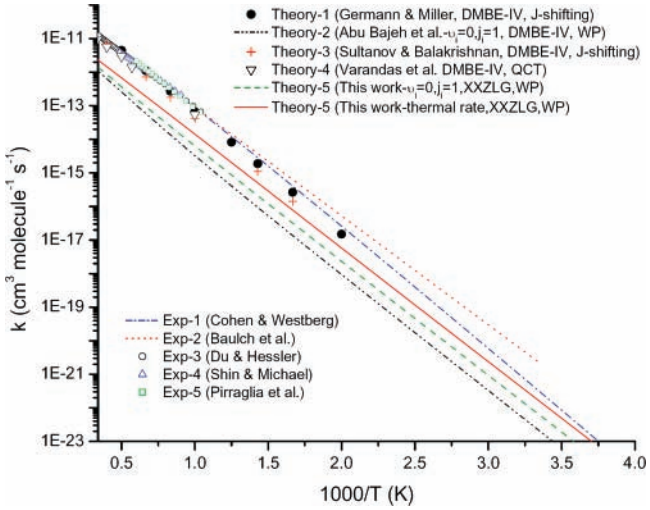

Figure 7. Temperature dependence of the initial state-specified or thermal rate constants calculated on the XXZLG PES using the wavepacket method. Also included are the experimental results of Cohen and Westberg (dash-dotted line),[3] Baulch et al. (dotted line),[7] Du and Hessler (open circles),[4] Shin and Michael (open triangles),[5] and Pirraglia et al. (open squares),[6] as well as theoretical results on the DMBE IV PES of Germann and Miller (solid circles),[15] Goldfield and Meijer (dash-dotted line),[39] Sultanov and Balakrishnan (crosses),[18] and Varandas (open triangles).[20]

It is interesting to note that our earlier $J = 0$ work suggested that excitation of either the rotational or the vibrational has a limited impact on the reactivity.[60] A similar conclusion was reached in the $J = 0$ quantum scattering study on the DMBE IV PES.[32] However, the ICS results reported here clearly indicate that the conclusion based on the $J = 0$ partial wave is premature. This is understandable from the opacity function in Figure 2 because the $J = 0$ contribution to the ICS is very small.

G. Rate Constant. Because of its importance in combustion chemistry, the thermal rate constant for the title reaction has been measured extensively in a wide temperature range,[3−6] and consensus exists.[7,8] In addition, the rate constant has also been calculated using several theoretical methods,[9−13,15−23] although none at the level of the current work. Our quantum rate constant should provide a stringent test of the ab initio PES and the dynamic model used to calculate this quantity.

Due to the endothermic nature of the title reaction, the rate constant becomes significant only at very high temperatures. In fact, its temperature dependence is known to be of the Arrhenius type, namely, increasing exponentially with the temperature. To converge the rate constant up to 3000 K, the ICS is needed up to the collision energy of 2.0 eV. In addition, many of the reactant internal states are populated at such temperatures. At 3000 K, for example, the equilibrium populations of the first three vibrational states of O_2 are 0.52, 0.25, and 0.12, respectively. At this point, it is still not possible to compute the thermal rate constant based on the Boltzmann average of all rovibrational states of O_2. Rather, we will present an approximate rate constant based on the thermal average of the O_2 vibrational states only because our results in Figure 6 showed a significant vibrational enhancement. On the other hand, we assume that the rotational excitation has little effect on the reactivity because of the lack of data for highly excited O_2 rotational states. The validity of the latter approximation certainly needs further investigation.

In Figure 7, both the initial state-specific and vibrationally averaged rate constants are compared with experimental and previous theoretical data. These rate constants were calculated

using eq 16 from the initial state-specific ICSs, whose calculations have been discussed in previous subsections. It is clear that the theoretical results are lower than the experimental values over the entire temperature range. The Boltzmann average over the reactant vibrational states helps to narrow the theory−experiment gap, but it is still not possible to reach a satisfactory agreement. On the other hand, it is interesting to note that the Arrhenius slope of the calculated rate constants is very similar to its experimental counterpart, indicating similar effective barriers. The calculated rate constant has an effective barrier of 0.667 eV, which is the same as the quantum endothermicity of the XXZLG PES. This can be compared with 0.644 eV in the experimental consensus summarized by Baulch et al.[7]

Before we speculate on the origin of the experiment−theory discrepancies, let us first comment on the comparison among various theoretical results. Since the quantum model of Goldfield and Meijer[36,37] has essentially the same KEO as ours, a direct comparison with our results could shed light on the differences due to the PES. To this end, the initial state ($v_i = 0, j_i = 1$)-specified rate constant obtained from the ICS of these authors[38] is compared in Figure 7 with that reported here. It is clear that the rate constant on the XXZLG PES is significantly larger and closer to the experimental data. The better agreement with experiment can be attributed to the improved PES, particularly the smaller endothermicity.

It is more difficult to assess the accuracy of other quantum results on the DMBE IV PES,[14−18] which seem to agree quite well with the experiment. In Figure 7, the results of Germann and Miller[15] and those of Sultanov and Balakrishnan[18] are displayed. These results were obtained using the *J*-shifting model. As shown in Figure 3, the overestimation of the rate constant by the *J*-shifting model is quite significant and may contribute to the fortuitous agreement in Figure 7. On the other hand, these calculations were based on the cumulative reaction probability, which includes all of the reactant states, whereas our results did not include all reactant rotational states.

Interestingly, the QCT results of Varandas et al. on the DMBE IV PES[20] shown in the same figure are in quite good agreement with the experimental values at high temperatures. We note that the QCT model included all accessible internal states of the reactant because the sampling was performed under thermal conditions. As a result, the vibrational enhancement of the reactivity should have been included, albeit classically. On the other hand, the QCT results contain significant uncertainties with regard to the precise treatment of the ZPE. The data we included in Figure 7 were obtained using the IEQMT (internal energy quantum mechanical threshold) protocol, which discards trajectories that have insufficient internal energy to exit the OH + O channel.[20] Its validity is difficult to assess, particularly at low temperatures where some discarded trajectories might gain sufficient energy to reach the product asymptote if they are allowed to evolve for a longer time. As shown in Figure 4, however, this particular protocol (IEQMT) for treating the OH ZPE overestimates the quantum ICS on the DMBE IV PES, which was reasonably tracked by the VEQMT protocol. Unfortunately, the VEQMT rate constant has not been reported.

Therefore, what are the possible sources of errors in our theoretical results? First, there is always the possibility that the ab initio potential may still not be sufficiently accurate. This is possible because the radical nature of the system makes the accurate determination of the global PES extremely difficult. A particularly vulnerable region is the OH + O product channel, which dominates the endothermic reaction. As discussed extensively in the literature,[12,28,56,85] this channel has a linear van der Waals well, which converts to the chemically bonded HO_2 well through a submerged barrier energetically below the OH + O asymptote. This "reef" structure becomes dominant at large *J* values. Incidentally, a similar "reef" structure also exists in the $O + O_2$ system,[87] where the rate constant was also found to underestimate the experimental values.[88,89] There, it has been shown that the rate constant is very sensitive to the reef region of the PES.[88] Too high of a submerged barrier will significantly attenuate the rate constant. Very recently, we carried out some preliminary icMRCI calculations with the AV5Z basis set in this region (C. Xu and D. Xie, private communications). The convergence with respect to the size of the basis set seems to be quite satisfactory.

Second, there are still dynamic approximations that might significantly affect the rate constant. For example, the higher rotational states of the O_2 reactant have not been explicitly considered in our model, although a dramatic increase of reactivity originating from reactant rotational excitation is unlikely. The most effective strategy to remedy this deficiency is probably to calculate the cumulative reaction probability and its dependence on the energy. Unlike several previous studies in which the $J > 0$ cases were treated with approximate quantum models,[14−18] however, a fully Coriolis-coupled method should be implemented.

Third, nonadiabatic coupling, which is not included in this work, could be important in both strongly interacting regions and the asymptotes. For example, the Renner−Teller coupling between the ground (X^2A'') and excited (A^2A') electronic states of HO_2 can cause nonadiabatic transitions near linearity. The latter correlates to the same OH + O asymptote as the former, although its reactant asymptote corresponds to an excited oxygen state.[53] In addition, there are also conical intersections above the reaction threshold.[53] The study of Kendrick and Pack has shown that the geometric phase effects around these conical intersections are quite large in this system, even at low collision energies.[41] Finally, there might also be strong nonadiabatic couplings in the asymptotic regions,[42,43] which might alter the reactivity.

Finally, there are possible experimental uncertainties. Although the measured rate constants for the title reaction are quite consistent,[8] several authors have suggested that the excited $O_2(^1\Delta_g)$ might be involved under the experimental conditions.[4,46] The $H + O_2(^1\Delta_g)$ reaction leads to the same products as those of the title reaction, and the corresponding electronic state (A^2A') is nonadiabatically coupled to the ground (X^2A'') electronic state of HO_2.

IV. Conclusions

In this work, we carried out accurate quantum wavepacket calculations for the title reaction using the XXZLG PES based on high-level ab initio calculations. The major conclusions of this study are summarized as follows.

(i) The reaction probabilities are highly oscillatory, particularly at low collision energies, but the oscillations diminish as energy increases. The direct channel observed in the DMBE IV PES is probably an artifact because it is absent on the ab initio XXZLG PES. At high *J* values, the reaction probability typically has a higher reaction threshold and increases monotonically with the energy. It is also observed that the sharp resonance structures diminish with increasing *J*.

(ii) Due to the barrierless nature of the title reaction, a large number of partial waves are needed to converge the cross sections. The excitation function increases relatively smoothly

with the collision energy as the resonance structures in the reaction probabilities are effectively washed out by partial wave summation.

(iii) The popular CS approximation is inadequate for the title reaction because the floppy HO_2 complex renders facile Coriolis coupling. The *J*-shifting model is also inappropriate due to the inherent lack of a transition state and was found to substantially overestimate the reactivity.

(iv) The reactant vibrational excitation was found to enhance the reactivity, presumably by helping the system to overcome the final O−O bond cleavage. On the other hand, the influence of the reactant rotation is less clear. Our results indicate that for low j_i values, the impact on the reactivity is limited. However, its effect for high j_i states requires further investigation.

(v) Direct comparison with previous quantum results of Goldfield and Meijer on the DMBE IV PES suggests that the new XXZLG PES yields a better agreement with experiment. Since essentially the same exact KEOs were used in the two quantum studies, the better agreement can be attributed to the improved PES, particularly the smaller endothermicity. Given the limited information available during the construction of the DMBE PES, however, the semiempirical PES has proven remarkably resilient for the title reaction.

(vi) The calculated ICS and rate constant still underestimate the available experimental data. The most likely factors include the inaccuracies of the PES, the neglect of highly excited O_2 rotational states, and nonadiabatic interactions.

Despite its deceptively simple appearance, a complete understanding of the dynamics of the title reaction remains elusive. The latest assault on this problem, represented by the current work, included the state-of-the-art ab initio calculation of the global PES and a nearly exact dynamic treatment of the reactive scattering. However, this level of theory is apparently still insufficient for reproducing the experimental rate constant and integral cross section. As a result, future dynamic studies have to include several features neglected in our model, such as nonadiabatic couplings. In the mean time, we also hope that our theoretical work will stimulate more experimental investigations on the reaction dynamics of this prototypical system.

Acknowledgment. This work was supported by the U.S. Department of Energy (DE-FG02-05ER15694, S.Y.L. and H.G.). Z.G.S. and S.Y.L. gratefully acknowledge support from a Singapore Ministry of Education Research Grant. D.H.Z. acknowledges the support of the Knowledge Innovation Program of the Chinese Academy of Sciences (Grant DICP R200402 and Y200601) and of the National Natural Science Foundation of China (Grant No. 20688301). P.H. acknowledges support from the Institut du Développement des Ressources en Informatique Scientifique (IDRIS) in Orsay (France). D.X. was supported by the National Natural Science Foundation of China (Grant Nos. 20725312 and 20533060) and the Ministry of Science and Technology (2007CB815201). Parts of the calculations were performed on DOE's NERSC facility. H.G. thanks Evi Goldfield and Anthony Meijer for many useful discussions.

References and Notes

(1) Miller, J. A.; Kee, R. J.; Westbrook, C. K. *Annu. Rev. Phys. Chem.* **1990**, *41*, 345.
(2) Litorja, M.; Rusic, B. *J. Electron Spectrosc. Relat. Phenom.* **1998**, *97*, 131.
(3) Cohen, N.; Westberg, K. R. *J. Phys. Chem. Ref. Data* **1983**, *12*, 531.
(4) Du, H.; Hessler, J. P. *J. Chem. Phys.* **1992**, *96*, 1077.
(5) Shin, K. S.; Michael, J. V. *J. Chem. Phys.* **1991**, *95*, 262.
(6) Pirraglia, A. N.; Michael, J. V.; Sutherland, J. W.; Klemm, R. B. *J. Phys. Chem.* **1989**, *93*, 282.
(7) Baulch, D. L.; Cobos, C. J.; Cox, R. A.; Frank, P.; Hayman, G.; Just, T.; Kerr, J. A.; Murrells, T.; Pilling, M. J.; Troe, J.; Walker, R. W.; Warnatz, J. *J. Phys. Chem. Ref. Data* **1994**, *23*, 847.
(8) Miller, J. A.; Pilling, M. J.; Troe, J. *Proc. Combust. Inst.* **2005**, *30*, 43.
(9) Rai, S. N.; Truhlar, D. G. *J. Chem. Phys.* **1983**, *79*, 6046.
(10) Yang, C.-Y.; Klippenstein, S. J. *J. Chem. Phys.* **1995**, *103*, 7287.
(11) Miller, J. A.; Garrett, B. C. *Int. J. Chem. Kinet.* **1997**, *29*, 275.
(12) Harding, L. B.; Maergoiz, A. I.; Troe, J.; Ushakov, V. G. *J. Chem. Phys.* **2000**, *113*, 11019.
(13) Lin, S. Y.; Rackham, E. J.; Guo, H. *J. Phys. Chem. A* **2006**, *110*, 1534.
(14) Leforestier, C.; Miller, W. H. *J. Chem. Phys.* **1994**, *100*, 733.
(15) Germann, T. C.; Miller, W. H. *J. Phys. Chem. A* **1997**, *101*, 6358.
(16) Skinner, D. E.; Germann, T. C.; Miller, W. H. *J. Phys. Chem. A* **1998**, *102*, 3828.
(17) Viel, A.; Leforestier, C.; Miller, W. H. *J. Chem. Phys.* **1998**, *108*, 3489.
(18) Sultanov, R. A.; Balakrishnan, N. *J. Phys. Chem. A* **2004**, *108*, 8759.
(19) Miller, J. A. *J. Chem. Phys.* **1981**, *74*, 5120.
(20) Varandas, A. J. C.; Brandao, J.; Pastrana, M. R. *J. Chem. Phys.* **1992**, *96*, 5137.
(21) Harding, L. B.; Troe, J.; Ushakov, V. G. *Phys. Chem. Chem. Phys.* **2000**, *2*, 631.
(22) Troe, J.; Ushakov, V. G. *J. Chem. Phys.* **2001**, *115*, 3621.
(23) Teitelbaum, H.; Caridade, P. J. S. B.; Varandas, A. J. C. *J. Chem. Phys.* **2004**, *120*, 10483.
(24) Dochovic, R. J.; Parker, M. A. *J. Phys. Chem. A* **2005**, *109*, 5883.
(25) Nyman, G.; Davidsson, J. *J. Chem. Phys.* **1990**, *92*, 2415.
(26) Varandas, A. J. C. *J. Chem. Phys.* **1993**, *99*, 1076.
(27) Miller, J. A. *J. Chem. Phys.* **1986**, *84*, 6170.
(28) Pastrana, M. R.; Quintales, L. A. M.; Brandao, J.; Varandas, A. J. C. *J. Phys. Chem.* **1990**, *94*, 8073.
(29) Honvault, P.; Lin, S. Y.; Xie, D.; Guo, H. *J. Phys. Chem. A* **2007**, *111*, 5349.
(30) Zhang, D. H.; Zhang, J. Z. H. *J. Chem. Phys.* **1994**, *101*, 3671.
(31) Kendrick, B.; Pack, R. T. *Chem. Phys. Lett.* **1995**, *235*, 291.
(32) Pack, R. T.; Butcher, E. A.; Parker, G. A. *J. Chem. Phys.* **1995**, *102*, 5998.
(33) Pack, R. T. *J. Chem. Phys.* **1974**, *60*, 633.
(34) McGuire, P.; Kouri, D. J. *J. Chem. Phys.* **1974**, *60*, 2488.
(35) Bowman, J. M. *J. Phys. Chem.* **1991**, *95*, 4960.
(36) Meijer, A. J. H. M.; Goldfield, E. M. *J. Chem. Phys.* **1998**, *108*, 5404.
(37) Meijer, A. J. H. M.; Goldfield, E. M. *J. Chem. Phys.* **1999**, *110*, 870.
(38) Goldfield, E. M.; Meijer, A. J. H. M. *J. Chem. Phys.* **2000**, *113*, 11055.
(39) Abu, Bajeh, M.; Goldfield, E. M.; Hanf, A.; Kappel, C.; Meijer, A. J. H. M.; Volpp, H.-R.; Wolfrum, J. *J. Phys. Chem. A* **2001**, *105*, 3359.
(40) Bargeuno, P.; Gonzalez-Lezana, T.; Larregaray, P.; Bonnet, L.; Rayez, J.-C. *Phys. Chem. Chem. Phys.* **2007**, *9*, 1127.
(41) Kendrick, B.; Pack, R. T. *J. Chem. Phys.* **1997**, *106*, 3519.
(42) Graff, M. M.; Wagner, A. F. *J. Chem. Phys.* **1990**, *92*, 2423.
(43) Maergoiz, A. I.; Nikitin, E. E.; Troe, J.; Ushakov, V. G. Asymptotic Interactions between Open Shell Partners in Low Temperature Complex Formation: The H + O_2 and O + OH systems. In *Theory of Chemical Reaction Dynamics*; Lagana, A., Lendvay, G., Eds.; Kluwer: Dordrecht, The Netherlands, 2004; p 21.
(44) Kleinermanns, K.; Wolfrum, J. *Chem. Phys. Lett.* **1984**, *104*, 157.
(45) Jacobs, A.; Volpp, H. R.; Wolfrum, J. *Chem. Phys. Lett.* **1991**, *177*, 200.
(46) Kessler, K.; Kleinermanns, K. *J. Chem. Phys.* **1992**, *97*, 374.
(47) Melius, C. F.; Blint, R. J. *Chem. Phys. Lett.* **1979**, *64*, 183.
(48) Varandas, A. J. C.; Brandao, J. *Mol. Phys.* **1986**, *57*, 387.
(49) Varandas, A. J. C.; Brandao, J.; Quintales, L. A. M. *J. Phys. Chem.* **1988**, *92*, 3732.
(50) Walch, S. P.; Rohlfing, C. M.; Melius, C. F.; Baushlicher, C. W. *J. Chem. Phys.* **1988**, *88*, 6273.
(51) Walch, S. P.; Duchovic, R. J. *J. Chem. Phys.* **1991**, *94*, 7068.
(52) Barclay, V. J.; Dateo, C. E.; Hamilton, I. P. *J. Chem. Phys.* **1994**, *101*, 6766.
(53) Kendrick, B.; Pack, R. T. *J. Chem. Phys.* **1995**, *102*, 1994.
(54) Dai, J.; Zhang, J. Z. H. *J. Phys. Chem.* **1997**, *100*, 6898.
(55) Groenenboom, G. C. *J. Chem. Phys.* **1998**, *108*, 5677.
(56) Xu, C.; Xie, D.; Zhang, D. H.; Lin, S. Y.; Guo, H. *J. Chem. Phys.* **2005**, *122*, 244305.
(57) Xie, D.; Xu, C.; Ho, T.-S.; Rabitz, H.; Lendvay, G.; Lin, S. Y.; Guo, H. *J. Chem. Phys.* **2007**, *126*, 074315.
(58) Lin, S. Y.; Xie, D.; Guo, H. *J. Chem. Phys.* **2006**, *125*, 091103.

(59) Xu, C.; Jiang, B.; Xie, D.; Farantos, S. C.; Lin, S. Y.; Guo, H. *J. Phys. Chem. A* **2007**, *111*, 10353.
(60) Lin, S. Y.; Guo, H.; Honvault, P.; Xie, D. *J. Phys. Chem. B* **2006**, *110*, 23641.
(61) Hankel, M.; Smith, S. C.; Meijer, A. J. H. M. *J. Chem. Phys.* **2007**, *127*, 064316.
(62) Honvault, P.; Launay, J.-M. In *Theory of Chemical Reaction Dynamics*; Lagana, A., Lendvay, G., Eds.; Kluwer: Dordrecht, The Netherlands, 2004; p 187.
(63) Zhang, J. Z. H. *Theory and Application of Quantum Molecular Dynamics*; World Scientific: Singapore, 1999.
(64) Yuan, K.; Cheng, Y.; Liu, X.; Harich, S.; Yang, X.; Zhang, D. H. *Phys. Rev. Lett.* **2006**, *96*, 103202.
(65) Guo, H. Chebyshev Propagation and Applications to Scattering Problems. In *Theory of Chemical Reaction Dynamics*; Lagana, A., Lendvay, G., Eds.; Kluwer: Dordrecht, The Netherlands, 2004; p 217.
(66) Mandelshtam, V. A.; Taylor, H. S. *J. Chem. Phys.* **1995**, *102*, 7390.
(67) Mandelshtam, V. A.; Taylor, H. S. *J. Chem. Phys.* **1995**, *103*, 2903.
(68) Tal-Ezer, H.; Kosloff, R. *J. Chem. Phys.* **1984**, *81*, 3967.
(69) Chen, R.; Guo, H. *J. Chem. Phys.* **1996**, *105*, 3569.
(70) Gray, S. K.; Balint-Kurti, G. G. *J. Chem. Phys.* **1998**, *108*, 950.
(71) Huang, Y.; Kouri, D. J.; Hoffman, D. K. *Chem. Phys. Lett.* **1994**, *225*, 37.
(72) Huang, Y.; Kouri, D. J.; Hoffman, D. K. *J. Chem. Phys.* **1994**, *101*, 10493.
(73) Althorpe, S. C. *J. Chem. Phys.* **2001**, *114*, 1601.
(74) Lin, S. Y.; Guo, H. *Phys. Rev. A* **2006**, *74*, 022703.
(75) Light, J. C.; Carrington, T., Jr. *Adv. Chem. Phys.* **2000**, *114*, 263.
(76) Lin, S. Y.; Guo, H. *J. Phys. Chem. A* **2004**, *108*, 2141.
(77) Condon, E. U.; Shortley, G. H. *The Theory of Atomic Spectra*; Cambridge: London, 1964.
(78) Zare, R. N. *Angular Momentum*; Wiley: New York, 1988.
(79) Corey, G. C.; Lemoine, D. *J. Chem. Phys.* **1992**, *97*, 4115.
(80) Corey, G. C.; Tromp, J. W. *J. Chem. Phys.* **1995**, *103*, 1812.
(81) Lin, S. Y.; Guo, H. *J. Chem. Phys.* **2003**, *119*, 11602.
(82) Meijer, A. J. H. M.; Goldfield, E. M.; Gray, S. K.; Balint-Kurti, G. G. *Chem. Phys. Lett.* **1998**, *293*, 270.
(83) Messiah, A. *Quantum Mechanics*; Wiley: New York, 1968.
(84) Lin, S. Y.; Guo, H. *J. Chem. Phys.* **2006**, *124*, 031101.
(85) Xu, C.; Xie, D.; Honvault, P.; Lin, S. Y.; Guo, H. *J. Chem. Phys.* **2007**, *127*, 024304.
(86) Evans, M. G.; Polanyi, M. *Trans. Faraday Soc.* **1939**, *35*, 178.
(87) Siebert, R.; Fleurat-Lessard, P.; Schinke, R.; Bittererova, M.; Farantos, S. C. *J. Chem. Phys.* **2002**, *116*, 9749.
(88) Fleurat-Lessard, P.; Grebenshchikov, S. Y.; Siebert, R.; Schinke, R.; Halberstadt, N. *J. Chem. Phys.* **2003**, *118*, 610.
(89) Lin, S. Y.; Guo, H. *J. Phys. Chem. A* **2006**, *110*, 5305.